Ultrafast Transient Terahertz Conductivity of Monolayer MoS_2 and WSe_2 Grown by Chemical Vapor Deposition

Callum J. Docherty,[†] Patrick Parkinson,[†] Hannah J. Joyce,[†] Ming-Hui Chiu,[‡] Chang-Hsiao Chen,[§] Ming-Yang Lee,[§] Lain-Jong Li,[‡] Laura M. Herz,[†] and Michael B. Johnston*[,†]

[†]Department of Physics, University of Oxford, Clarendon Laboratory, Parks Road, Oxford OX1 3PU, U.K., [‡]Physical Science and Engineering Division, King Abdullah University of Science and Technology, Thuwal 23955-6900, Kingdom of Saudi Arabia, and [§]Institute of Atomic and Molecular Sciences, Academia Sinica, Taipei 115, Taiwan

ABSTRACT We have measured ultrafast charge carrier dynamics in monolayers and trilayers of the transition metal dichalcogenides MoS_2 and WSe_2 using a combination of time-resolved photoluminescence and terahertz spectroscopy. We recorded a photoconductivity and photoluminescence response time of just 350 fs from CVD-grown monolayer MoS_2, and 1 ps from trilayer MoS_2 and monolayer WSe_2. Our results indicate the potential of these materials as high-speed optoelectronic materials.

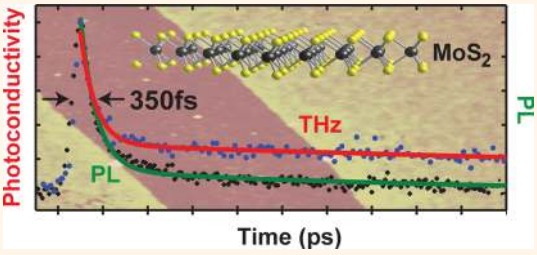

KEYWORDS: transition metal dichalcogenide · CVD · molybdenum disulfide · tungsten diselenide · ultrafast · terahertz conductivity · photoluminescence

For the past three decades, technological advances toward terahertz speed electronic and optoelectronic devices have relied on the staple materials of low-temperature grown gallium arsenide (LT-GaAs) and ion implanted semiconductors.[1−5] The combination of high initial mobility and rapid charge lifetimes required for ultrafast devices is achieved in these materials by introducing trapping sites into the bulk material.[1,6−8] The emergence of new two-dimensional materials,[9] however, offers the prospect of novel, cheap materials for high speed applications, without the need for difficult ion implantation procedures.

Transition metal dichalcogenides (TMDs) consist of transition metal atoms covalently bonded to chalcogens (S, Se or Te) to form atomic trilayers.[10−13] The trilayers stack *via* weak van der Waals interactions to form a 3-dimensional solid. TMDs have the potential to become the building blocks of a wide range of future electronic devices as they act as semiconductors, semimetals or metals depending on the choice of transition metal.[12]

Molybdenum disulfide (MoS_2) and tungsten diselenide (WSe_2) are semiconducting TMDs that have been well studied[10,12,14] in their *multilayer (3D)* form. MoS_2 is extensively used in industry as a dry lubricant[15] and as a catalyst for the hydrodesulphurisation of petroleum.[16] Only recently has truly *monolayer (2D)* MoS_2 been experimentally realized, exposing a wealth of new photophysics.[9,17−21] For instance, while MoS_2 is an indirect bandgap semiconductor in the bulk (multilayer) form, it has a direct bandgap as a monolayer and thus exhibits greatly enhanced photoluminescence yield.[17,18] Furthermore, negative trions, which are quasiparticles consisting of two electrons and a hole, have been discovered in monolayer MoS_2.[22,23]

As a result of these discoveries, MoS_2 is already showing promise for use in electronic and photonic devices,[11] such as field effect transistors,[9,24−28] photodiodes[29] and memory applications.[30] However, the observed low electron mobility in MoS_2[31−33] is problematic for the further development of

* Address correspondence to m.johnston@physics.ox.ac.uk.

Received for review March 21, 2014 and accepted October 27, 2014.

Published online October 27, 2014
10.1021/nn5034746

these devices, particularly those that require high frequency operation. While the reason for low electron mobility in MoS_2[31−33] is a matter of debate, it is clear that a better understanding of the fundamental optical and electrical properties of TMDs is required in order to realize high performance devices.

The predominantly n-type nature of MoS_2 makes the development of electronic devices requiring p-type charge transport challenging. Another TMD, tungsten diselenide (WSe_2) offers a possible solution to this problem as it is an intrinsic semiconductor possessing ambipolar charge transport.[34,35] WSe_2 shows many of the properties that make MoS_2 interesting, becoming a direct gap semiconductor in its monolayer form, and exhibiting trions.[36] Thus, WSe_2 in its own right and layers of WSe_2 combined with MoS_2 show promise as key materials for future optoelectronic devices. However, to date there have been few studies on the photophysics of WSe_2.[36,37]

Most studies and devices reported to date have utilized mechanically exfoliated MoS_2 and WSe_2, using the "scotch tape" method pioneered in early graphene research.[38−41] Unfortunately this method of producing monolayers of layered materials is not well suited to large-scale industrial production. Recently, MoS_2 and WSe_2 have been produced using chemical vapor deposition (CVD).[35,42−44] This bottom-up technique is compatible with current commercial production technologies and is also the method currently favored for the production of graphene.[45]

Previous time-resolved photophysical studies of MoS_2 have utilized photoluminescence (PL) spectroscopy,[46] electroluminescence,[47] optical pump−probe spectroscopy[48] and transient absorption[49] to investigate exciton dynamics in mechanically exfoliated few- and monolayer MoS_2. These studies generally observed a relaxation of photoexcited species on two distinct time scales: a fast, few picosecond decay followed by a slower component on the scale of several tens of picoseconds. However, these studies were not able to probe directly the conductive species that are of interest for optoelectronic devices. To our knowledge, no time-resolved studies of monolayer WSe_2 have so far been published.

Here, we present studies of monolayer and trilayer CVD-grown MoS_2 and WSe_2 using terahertz time domain spectroscopy (THz TDS) and PL spectroscopy. Together, these techniques allowed us to observe the behavior of free carriers and excitons in photoexcited MoS_2. We observed a photoconductivity response in CVD-grown MoS_2 of just 350 fs. Such an ultrafast response time is particularly promising for the future use of TMDs in high-speed (>1 THz) photodetectors, emitters and transistors. However, many challenges still remain to realize such devices, such as obtaining materials with very high charge carrier mobility. The possibility of tuning the conductivity lifetime in MoS_2 *via* substrate interactions and film thickness offers the option of producing cost-effective optoelectronic materials with tunable charge carrier lifetimes. Further measurements suggest the observation of trions in monolayer MoS_2 and WSe_2.

Sample Preparation and Characterization. Predominantly monolayer MoS_2, trilayer MoS_2, and monolayer WSe_2 films were grown directly onto sapphire substrates by chemical vapor deposition. More detail about the growth methodologies may be found in refs 42−44 and in the Methods section.

The number of layers in each sample was determined by Raman spectroscopy and atomic force microscopy (AFM). Figure 1 (b) and (f) show the Raman spectra of the monolayer and trilayer samples, respectively. The splitting between the E^1_{2G} and A_{1G} peaks in the Raman spectrum of the monolayer (trilayer) MoS_2 was 18 cm^{-1} (23 cm^{-1}), which is indicative of single (tri)layer growth.[50] The AFM images of intentionally scratched samples are presented in Figure 1 (c), (g), and (k). They show step heights of 0.7, 2.3 and 0.73 nm, which confirm that the samples consist of monolayer MoS_2, trilayer MoS_2, and monolayer WSe_2, respectively. Figure 1 (d) and Figure 1 (h) show the optical transmission spectra of monolayer and trilayer MoS_2, respectively. The two absoprtion features at 1.89 and 2.04 eV are characteristic of MoS_2 and are known as the "A" and "B" excitions. Similarly, the features at 1.65 and 2.06 eV of Figure 1 (l) correspond to the "A" and "B" excitons of WSe_2.

Electron double layer transistors (EDLTs) were fabricated to assess the sheet charge carrier density in the layers. The MoS_2 layers were found to be predominately n-type, while the WSe_2 layers were found to be ambipolar (see Supporting Information Figures S1 and S2).

RESULTS

We used a combination of photoluminescence (PL) and THz conductivity spectroscopy to observe the dynamics of photoexcited charge species in the samples. Here we use the term "charge species" to refer to free electrons and holes as well as correlation between charges such as excitons, charged excitons (trions) and plasmons. PL is sensitive only to the subset of photoinjected charge species that recombine radiatively. In contrast THz conductivity spectroscopy is sensitive to any conductive or polarizable charge species independent of whether the excitation relaxes radiatively or nonradiatively.[51] Furthermore, THz spectra can be used to identify types of charge species and how they evolve on picosecond time scales. For example excitons, plasmons and free charges have distinct spectral signatures at THz frequencies.[52] Therefore, together time-resolved PL and THz spectroscopy allow complicated charge dynamics involving more than one type of charge species to be interpreted.

Figure 2a shows the photoluminescence recorded at 1.86 eV arising from monolayer MoS_2 as a function of time after photoexcitation with 3.0 eV photons. The energy of the absorbed photons are significantly

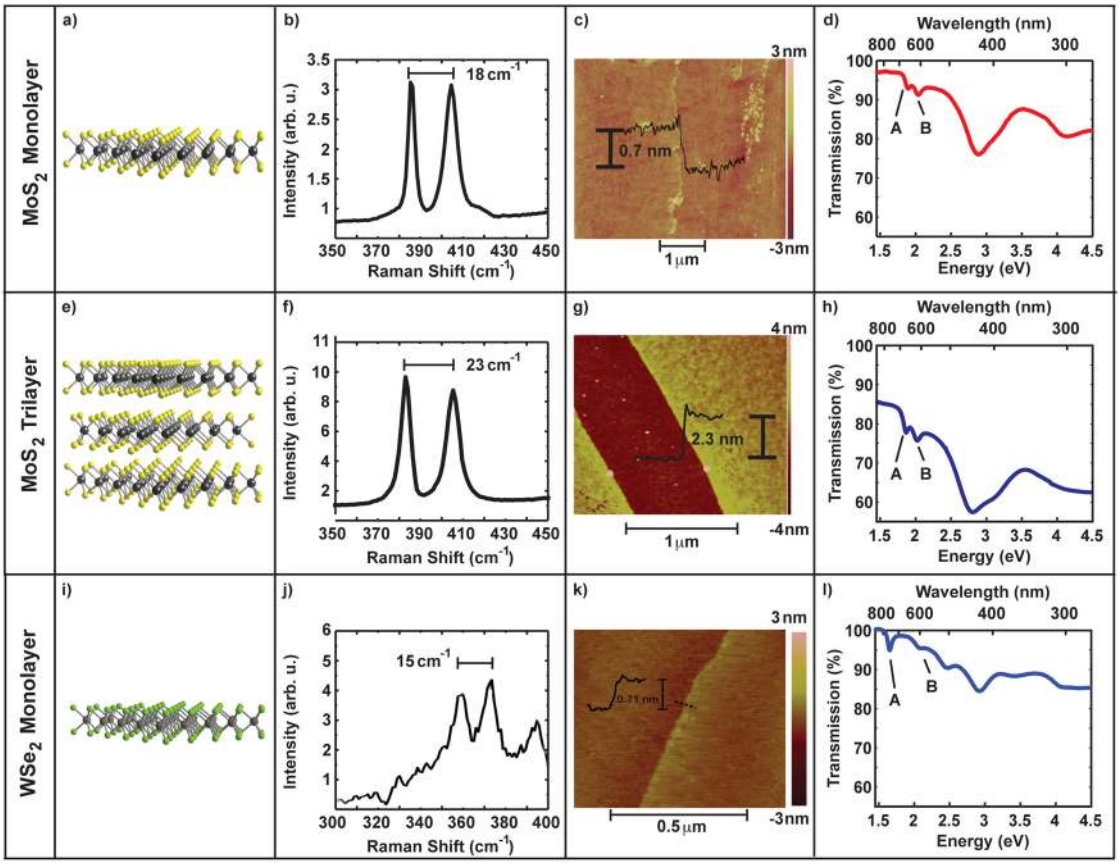

Figure 1. Characterization of monolayer MoS_2 (a–d), trilayer MoS_2 (e–h), and monolayer WSe_2 samples. (a), (e), (i) Schematic representation of the samples. (b), (f), (j) Raman spectroscopy of the samples. The splitting between the E^1_{2G} and A_{1G} peaks is indicative of layer number. (c), (g), (k) AFM images of the samples. Height profiles are overlaid at the position they were taken. The step heights again confirm the layer number identification. (d), (h), (l) Optical transmission spectrum of the samples. Absorption features associated with the "A" and "B" excitons are labeled.

above the MoS_2 bandgap and hence should photoinject electron–hole pairs with significant kinetic energy (*i.e.*, "hot" carriers). Overlaid on this graph is the THz photoconductivity $\Delta\sigma_{THz}(t)$ of the same sample as a function of time after photoexcitation with similar energy (3.1 eV) photons. The THz photoconductivity was found by measuring the change of transmission of the peak of the THz pulse through the sample after photoexcitation by a pump pulse.[51] Note that only the amplitude of the signal changed as a function of time after photoexcitation, not the phase. The full photoconductivity spectrum is discussed later (see Figure 5). The pump fluence dependence of this photoexcitation is linear, as shown in the Supporting Information. Photoexcitation of the sample leads to a sharp (instrument response limited) rise in both THz photoconductivity and PL emission followed by an ultrashort 350 fs exponential decay of both signals. The exponential decays of the photoconductivity and PL signals suggest that monomolecular charge recombination dominates over bimolecular recombination of electron–hole pairs.[53] The observed monomolecular recombination could result from exciton recombination, charge-carrier trapping or (if the system is doped) from recombination of minority charge carriers. After a few picoseconds the PL signal disappears; however, a significant persistent THz photoconductivity is still evident 10 ps after photoexcitation.

To understand more about the origin of the persistent photoconductivity in monolayer MoS_2 we also resonantly photoexcited the "A" and "B" excitons and recorded the THz conductivity and PL dynamics. Figure 2b shows that upon resonant photoexcitation the early time PL and $\sigma_{THz}(t)$ dynamics are remarkably similar to the case of above-bandgap photoexcitation. At later times (<3 ps) however the persistent photoconductivity signal is far less pronounced than for the nonresonant case and the PL is quenched even more effectively. There are a number of possible explanations for these observations. Nonresonant excitation may for example photoinject charge carriers to indirect-gap side valleys, leading to quenched PL but persistent conductivity. Alternatively, nonresonant excitation may lead to an increased probability of forming dark excitons *via* intersystem crossing, which would have a THz photoconductivity response without emitting PL.

Together, these results indicate that there is a rapid quenching of both PL and photoconductivity in

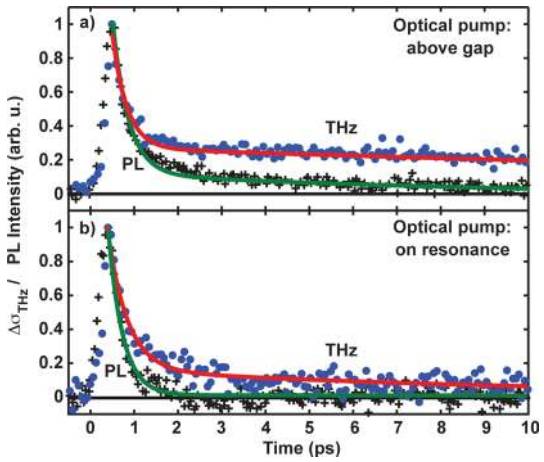

Figure 2. Photodynamics of monolayer MoS_2 measured by optical pump−THz probe spectroscopy and PL upconversion spectroscopy. (a) The blue circles show the normalized THz photoconductivity, $\Delta\sigma_{THz}$, of monolayer MoS_2 as a function of time after photoexcitation by 3.1 eV photons (absorbed fluence $\sim 7 \times 10^{13}$ cm^{-2}/pulse). The black crosses show the normalized PL emitted at 1.86 eV as a function of time after photoexcitation by 3 eV photons (absorbed fluence $\sim 6.9 \times 10^{12}$ cm^{-2}/pulse). Solid lines are biexponential fits to the data. (b) Similar $\Delta\sigma_{THz}$ (blue circles) and PL (black crosses) measurements following photoexcitation on resonance with the direct gap excitons (1.9 eV photons with absorbed fluence $\sim 1.2 \times 10^{14}$ cm^{-2} for $\Delta\sigma_{THz}$, and 2.1 eV photons with absorbed fluence $\sim 3.5 \times 10^{12}$ cm^{-2} for PL).

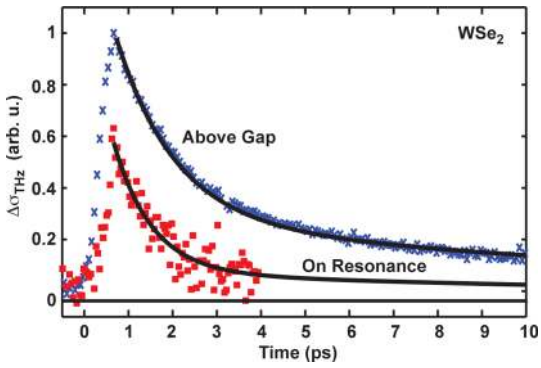

Figure 3. Normalized photodynamics of monolayer WSe_2 measured by optical pump-THz probe spectroscopy. The blue crosses show the THz photoconductivity of WSe_2, $\Delta\sigma_{THz}$, as a function of time after photoexcitation by 35 fs pulses of above-gap photons with energy of 3.1 eV. The absorbed photon fluence was $\sim 4.2 \times 10^{13}$ cm^{-2}/pulse. The red squares show $\Delta\sigma_{THz}$ of WSe_2 photoexcited resonantly with the "A" exciton at a photon energy of 1.65 eV. The fluence absorbed in the WSe_2 layer was $\sim 3.3 \times 10^{13}$ cm^{-2}/pulse. Solid lines are biexponential fits to the data.

monolayer MoS_2 within 350 fs photoexcitation. This quenching is independent of whether excitons are created resonantly or a hot electron−hole population is photoinjected into the sample. The fast quenching may be a result of (i) fast surface trapping, (ii) surface−substrate interactions for monolayer MoS_2, and/or (iii) extrinsic charge carrier mediated recombination.

To gain insight into the contribution of extrinsic charge carriers to the recombination dynamics, we compare the density of injected electron−hole pairs in our photoconductivity experiments with the areal concentration of extrinsic charge carriers (*i.e.*, doping level) in our MoS_2 monolayers. EDLTs fabricated from the MoS_2 monolayers were found to be n-type with sheet electron density of $2-3 \times 10^{13}$ cm^{-2} (Supporting Information Figure S1). In comparison, the maximum absorbed photon fluences in our photoconductivity experiments were significantly higher ($7-12 \times 10^{13}$ cm^{-2}). The exponential decay rate of photoconductivity quenching was found to be invariant as the absorbed fluence was lowered. Such invariance is expected for either trap or extrinsic carrier dominated quenching only under the condition that the absorbed fluence is significantly smaller than the areal trap or doping density.[54] Thus, we speculate that the recombination dynamics are probably dominated by an areal trap density higher than 12×10^{13} cm^{-2}.

Time resolved photocurrent measurements were also performed on monolayer WSe_2, which as found to be ambipolar (Supporting Information Figure S1). The THz photoconductivity of WSe_2 is presented in Figure 3. Above gap photoexcitation was provided by a 3.1 eV pump beam, as for the MoS_2 measurements. For excitation resonant with the excitons in WSe_2, however, a lower energy pump of 1.65 eV was used, matching the lower energy of the "A" exciton in WSe_2 compared to that in MoS_2.

As was observed for MoS_2, upon photoexcitation of WSe_2 by either pump energy, the THz photoconductivity rises sharply, but with a slower rise time than for MoS_2 ($\sim$700 fs compared to an instrument limited rise time of 350 fs in MoS_2). The photoconductivity then decays with a fast exponential lifetime of 1 ps followed by a slower fall over $\sim$15 ps. For both photoexcitation energies the time constants in WSe_2 are noticeably longer than those in monolayer MoS_2. A full understanding of the differences in rise and fall times between MoS_2 and WSe_2 is beyond the scope of this study, but these results provide a basis for future theoretical works.

In nanoscale materials the influence of surface trapping can be assessed by observing changes in transient photoconductivity as a function of the surface-area-to-volume ratio of the sample.[55,56] We compared the photoconductivity dynamics of *monolayer* MoS_2 with the *trilayer* sample to gauge the importance of the surface-area-to-volume ratio on conductivity dynamics. As can be seen in Figure 4 and the exponential fit parameters displayed in Table S1 of the Supporting Information, the photoconductivity decays three times slower in the trilayer samples compared with the monolayer. It is notable that even in high-quality bulk crystals of MoS_2, DC photoconductivity measurements are dominated by surface trapping effects.[57] Thus, for our CVD-grown monolayer samples we expect surface trapping to be the dominant mechanism of ultrafast PL and THz conductivity quenching.

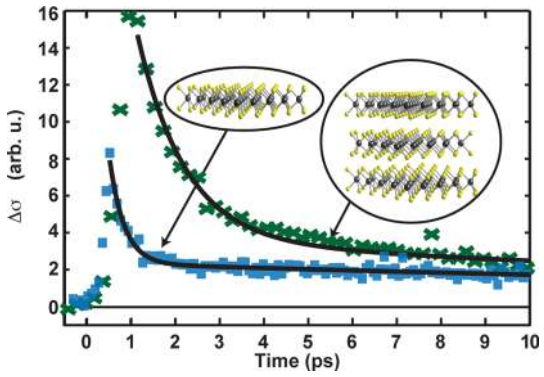

Figure 4. Comparison of THz photoconductivity, $\Delta\sigma_{THz}$, in trilayer (green crosses) and monolayer (blue squares) MoS_2 as a function of time after photoexcitation by 175 μJ cm^{-2} 35 fs pulses of 3.1 eV photons. The absorbed fluence of photons were $\sim 1.4 \times 10^{14}$ cm^{-2}/pulse in the trilayer sample and $\sim 7 \times 10^{13}$ cm^{-2}/pulse in the monolayer sample. Solid lines show biexponential fits to the data. Fit parameters are listed in Supporting Information Table 1. Additional reflections due to the thinness of the substrate have been removed from the trilayer data for clarity (see Supporting Information).

Further information can also be gained from the complex THz photoconductivity spectrum, $\Delta\sigma(\omega)$. In Figure 5 we present the photoinduced THz conductivity for mono and trilayer MoS_2 taken at 1.5 ps after photoexcitation, and for monolayer WSe_2 at 1 ps after photoexcitation. All three samples appear to have a small free-carrier (Drude type) response combined with stronger Lorentzian resonances (see Supporting Information Table S2). This tends to suggest the presence of a small component of free charge carriers in addition to excitonic species. Trilayer MoS_2, however, exhibits noticeably different behavior to both monolayer MoS_2 and WSe_2. The photoconductivity of trilayer MoS_2 appears to show a resonance far beyond the bandwidth of the experiment, consistent with the behavior expected from excitons of binding energy ~100 meV. In contrast, the monolayer samples show a resonance at ~15 meV. The solid lines in Figure 5 represent potential models of these data, detailed in the Supporting Information.

Recently trions, quasiparticles consisting of two electrons and a hole or two holes and an electron, have been observed in PL spectra from MoS_2 and WSe_2 with binding energies of 18 and 24 meV, respectively.[22,36] The similarity of these values to the monolayer resonance energies suggests the direct observation of trions in the monolayer samples. However, the signal-to-noise ratio in the spectrum is not high enough to draw firm conclusions.

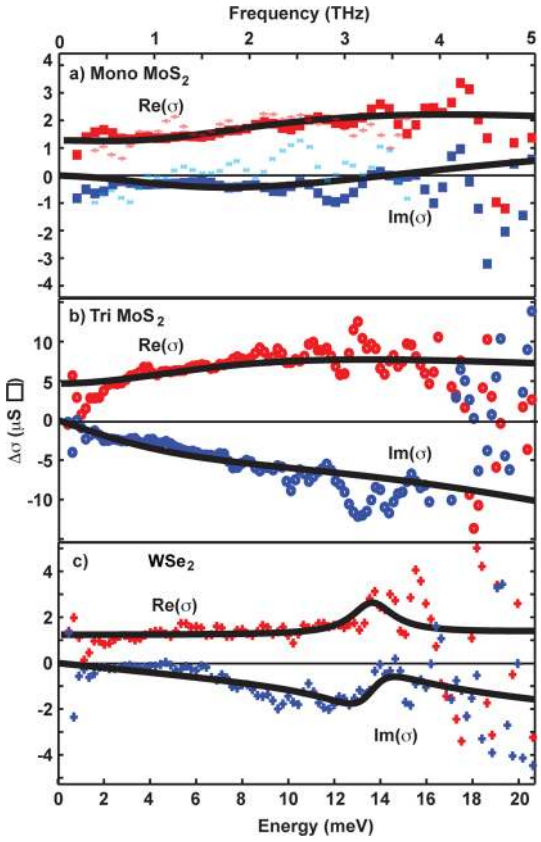

Figure 5. THz complex photoconductivity spectra, $\Delta\sigma(\nu)$. (a) Monolayer MoS_2 1.5 ps after photoexcitation with 3 eV (squares) and 1.9 eV (crosses) photons. A low energy resonance at ~18 meV (4.5 THz) is apparent. (b) Trilayer MoS_2, 1.5 ps after photoexcitation by 1.9 eV photons. (c) Monolayer WSe_2, 1 ps after photoexcitation on resonance with the WSe_2 "A" exciton at 1.65 eV. Solid lines show possible fits to the data, detailed in the Supporting Information.

CONCLUSION

In summary, we have observed ultrafast photoconductivity responses in monolayer MoS_2 and WSe_2, which we attribute to charge trapping at surface states. A monolayer semiconductor with such a fast response is likely to be a key component of future high-frequency optoelectronic devices including photoreceivers, emitters, modulators as well as microwave and THz switches. The low-cost and scalable CVD production of these monolayers, and their easy integration into devices, make them particularly attractive materials for such devices.

METHODS

Sample Preparation. Predominantly monolayer and trilayer MoS_2 films were grown directly onto sapphire substrates. Briefly, (0001)-oriented sapphire substrates (Tera Xtal technology Corp.) were cleaned with a H_2SO_4/H_2O_2 (70:30) solution at 100 °C for 1 h. For *monolayer* growth, the substrate was then placed at the center of a 2-in. tubular furnace on a quartz holder. Precursors of 0.3 g of MoO_3 (Sigma-Aldrich, 99.5%) in an Al_2O_3 crucible and S powder (Sigma-Aldrich, 99.5%) were placed at an upstream position in the reaction chamber. The furnace was first heated to 150 °C and annealed for 30 min with 70 sccm of Ar at 10 Torr, followed by heating at 650 °C for 10 min. The furnace was subsequently cooled slowly to room temperature.

Trilayers were grown by a two-step thermolysis of the precursor $(NH_4)_2MoS_4$.[44] The sapphire substrate was immersed in a solution of the $(NH_4)_2MoS_4$ precursor dissolved in 20 mL of dimethylformamide. The substrate was slowly removed from the solution, leaving a thin $(NH_4)_2MoS_4$ film, and baked at 120 °C for 30 min. A two-step annealing process was performed to transform the precursor film to trilayer MoS_2.

Monolayer WSe_2 was prepared similarly on sapphire substrates. WO_3 powders (0.3 g) were heated to 925 °C at a ramping rate of 25 °C/min with Se powder in the furnace. The sapphire substrates were put at the downstream side, where the Se and WO_3 vapors were delivered by an Ar/H_2 flowing gas (Ar = 80 sccm, H_2 = 20 sccm, chamber pressure = 1 Torr). After reaching 925 °C, the heating zone was kept for 15 min, and the furnace was then naturally cooled to room temperature. Additional details about the growth methodologies may be found in refs 42−44.

Photoluminescence Spectroscopy. Photoluminescence measurements were carried out using an 80 MHz 100 fs pulsed Ti:sapphire excitation source. For all experiments the excitation fluence was set to 15 $\mu J/cm^2$/pulse. Time-resolved photoluminescence was measured using photoluminescence up-conversion spectroscopy as described in ref 58.

THz Spectroscopy. An optical pump THz-TDS probe spectrometer was used to measure the photoconductivity $\Delta\sigma_{THz}(t,\nu)$ of MoS_2 and WSe_2 as a function of frequency ν and time t after photoexcitation. Details of the spectrometer and a description of how photoconductivity was extracted from the raw data has been described previously.[55,59] Briefly, the spectrometer was driven by a Ti:sapphire laser amplifier, which generated 35 fs duration, 0.8 mJ pulses of 800 nm light at 5 kHz repetition rate. THz probe pulses were generated by optical rectification in a 2 mm thick (110)-GaP crystal and detected *via* electro-optic sampling in a 0.2 mm-thick (110)-GaP crystal. A typical THz pulse can be seen in Supporting Information Figure S4. For the pump−probe measurements in Figures 2−4, the change in transmission due to photoexcitation of the peak of the THz electric field was measured, whereas for the photoconductivity spectra in Figure 5 the whole THz pulse was measured, with each part of the pulse measured at a fixed time after photoexcitation.[51] Samples were photoexcited by 35 fs laser pulses (typical fluence 175 $\mu J/cm^2$/pulse) at selected wavelengths using an optical parametric amplifier, or by frequency doubling pulses in a 0.2 mm-thick Type I BBO crystal. All measurements reported here were performed in a vacuum ($<10^{-3}$ mbar) at room temperature.

Conflict of Interest: The authors declare no competing financial interest.

Acknowledgment. We would like to thank A. Prabakaran and N. Grobert for performing Raman mapping measurments on the samples after the THz measurments were completed. The authors would like to thank the EPSRC (UK), Academia Sinica (IAMS and Nano program) and National Science Council Taiwan (NSC-99-2112-M-001-021-MY3) for financial support.

Supporting Information Available: detailing the pump fluence and pump energy dependence of the THz spectroscopy measurements, as well as information above removing reflections from the trilayer THz photoconductivity. This material is available free of charge *via* the Internet at http://pubs.acs.org.

REFERENCES AND NOTES

1. Smith, F. W.; Le, H. Q.; Diadiuk, V.; Hollis, M. A.; Calawa, A. R.; Gupta, S.; Frankel, M.; Dykaar, D. R.; Mourou, G. A.; Hsiang, T. Y. Picosecond GaAs-based Photoconductive Optoelectronic Detectors. *Appl. Phys. Lett.* **1989**, *54*, 890–892.
2. Nolte, D. D. Semi-insulating Semiconductor Heterostructures: Optoelectronic Properties and Applications. *J. Appl. Phys.* **1999**, *85*, 6259–6289.
3. Krotkus, A. Semiconductors for Terahertz Photonics Applications. *J. Phys. D: Appl. Phys.* **2010**, *43*, 273001.
4. Loka, H. S.; Benjamin, S. D.; Smith, P. W. E. Optical Characterization of Low-temperature-grown GaAs for Ultrafast All-optical Switching Devices. *IEEE J. Quantum Electron.* **1998**, *34*, 1426–1437.
5. Shen, Y. C.; Upadhya, P. C.; Linfield, E. H.; Beere, H. E.; Davies, A. G. Ultrabroadband Terahertz Radiation from Low-temperature-grown GaAs Photoconductive Emitters. *Appl. Phys. Lett.* **2003**, *83*, 3117–3119.
6. Ferguson, B.; Zhang, X.-C. Materials for Terahertz Science and Technology. *Nat. Mater.* **2002**, *1*, 26–33.
7. Castro-Camus, E.; Lloyd-Hughes, J.; Fu, L.; Tan, H. H.; Jagadish, C.; Johnston, M. B. An Ion-implanted InP Receiver for Polarization Resolved Terahertz Spectroscopy. *Opt. Express* **2007**, *15*, 7047–7057.
8. Mangeney, J. THz Photoconductive Antennas Made from Ion-bombarded Semiconductors. *J. Infrared, Millimeter, Terahertz Waves* **2012**, *33*, 455–473.
9. Novoselov, K. S.; Jiang, D.; Schedin, F.; Booth, T. J.; Khotkevich, V. V.; Morozov, S. V.; Geim, A. K. Two-dimensional Atomic Crystals. *Proc. Natl. Acad. Sci. U. S. A.* **2005**, *102*, 10451–10453.
10. Friend, R. H.; Yoffe, A. D. Electronic-properties of Intercalation Complexes of the Transition-metal Dichalcogenides. *Adv. Phys.* **1987**, *36*, 1–94.
11. Wang, Q. H.; Kalantar-zadeh, K.; Kis, A.; Coleman, J. N.; Strano, M. S. Electronics and Optoelectronics of Two-dimensional Transition Metal Dichalcogenides. *Nat. Nanotechnol.* **2012**, *7*, 699–712.
12. Chhowalla, M.; Shin, H. S.; Eda, G.; Li, L. J.; Loh, K. P.; Zhang, H. The Chemistry of Two-dimensional Layered Transition Metal Dichalcogenide Nanosheets. *Nat. Chem.* **2013**, *5*, 263–275.
13. Jariwala, D.; Sangwan, V. K.; Lauhon, L. J.; Marks, T. J.; Hersam, M. C. Emerging Device Applications for Semiconducting Two-dimensional Transition Metal Dichalcogenides. *ACS Nano* **2014**, *8*, 1102–1120.
14. Coehoorn, R.; Haas, C.; Degroot, R. A. Electronic-structure of $MoSe_2$, MoS_2, and WSe_2. II The Nature of the Optical Band-gaps. *Phys. Rev. B: Condens. Matter Mater. Phys.* **1987**, *35*, 6203–6206.
15. Kim, Y.; Huang, J. L.; Lieber, C. M. Characterization of Nanometer Scale Wear and Oxidation of Transition-metal Dichalcogenide Lubricants by Atomic Force Microscopy. *Appl. Phys. Lett.* **1991**, *59*, 3404–3406.
16. Karunadasa, H. I.; Montalvo, E.; Sun, Y. J.; Majda, M.; Long, J. R.; Chang, C. J. A Molecular MoS_2 Edge Site Mimic for Catalytic Hydrogen Generation. *Science* **2012**, *335*, 698–702.
17. Splendiani, A.; Sun, L.; Zhang, Y. B.; Li, T. S.; Kim, J.; Chim, C. Y.; Galli, G.; Wang, F. Emerging Photoluminescence in Monolayer MoS_2. *Nano Lett.* **2010**, *10*, 1271–1275.
18. Mak, K. F.; Lee, C.; Hone, J.; Shan, J.; Heinz, T. F. Atomically Thin MoS_2: A New Direct-gap Semiconductor. *Phys. Rev. Lett.* **2010**, *105*, 136805.
19. Yin, Z. Y.; Li, H.; Li, H.; Jiang, L.; Shi, Y. M.; Sun, Y. H.; Lu, G.; Zhang, Q.; Chen, X. D.; Zhang, H. Single-layer MoS_2 Phototransistors. *ACS Nano* **2012**, *6*, 74–80.
20. Choi, W.; Cho, M. Y.; Konar, A.; Lee, J. H.; Cha, G. B.; Hong, S. C.; Kim, S.; Kim, J.; Jena, D.; Joo, J.; *et al.* High-detectivity Multilayer MoS_2 Phototransistors with Spectral Response from Ultraviolet to Infrared. *Adv. Mater.* **2012**, *24*, 5832–5836.
21. Lopez-Sanchez, O.; Lembke, D.; Kayci, M.; Radenovic, A.; Kis, A. Ultrasensitive Photodetectors Based on Monolayer MoS_2. *Nat. Nanotechnol.* **2013**, *8*, 497–501.
22. Mak, K. F.; He, K. L.; Lee, C.; Lee, G. H.; Hone, J.; Heinz, T. F.; Shan, J. Tightly Bound Trions in Monolayer MoS_2. *Nat. Mater.* **2013**, *12*, 207–211.
23. Coleman, J. N.; Lotya, M.; O'Neill, A.; Bergin, S. D.; King, P. J.; Khan, U.; Young, K.; Gaucher, A.; De, S.; Smith, R. J.; *et al.* Two-dimensional Nanosheets Produced by Liquid Exfoliation of Layered Materials. *Science* **2011**, *331*, 568–571.
24. Wang, H.; Yu, L. L.; Lee, Y. H.; Shi, Y. M.; Hsu, A.; Chin, M. L.; Li, L. J.; Dubey, M.; Kong, J.; Palacios, T. Integrated Circuits Based on Bilayer MoS_2 Transistors. *Nano Lett.* **2012**, *12*, 4674–4680.

25. Radisavljevic, B.; Radenovic, A.; Brivio, J.; Giacometti, V.; Kis, A. Single-layer MoS_2 Transistors. *Nat. Nanotechnol.* **2011**, *6*, 147–150.
26. Alam, K.; Lake, R. K. Monolayer MoS_2 Transistors beyond the Technology Road Map. *IEEE Trans. Electron Devices* **2012**, *59*, 3250–3254.
27. Radisavljevic, B.; Whitwick, M. B.; Kis, A. Small-signal Amplifier Based On Single-layer MoS_2. *Appl. Phys. Lett.* **2012**, *101*, 043103.
28. Radisavljevic, B.; Kis, A. Mobility Engineering and a Metal-insulator Transition in Monolayer MoS_2. *Nat. Mater.* **2013**, *12*, 815–820.
29. Zhang, W. J.; Chuu, C. P.; Huang, J. K.; Chen, C. H.; Tsai, M. L.; Chang, Y. H.; Liang, C. T.; Chen, Y. Z.; Chueh, Y. L.; He, J. H.; *et al.* Ultrahigh-gain Photodetectors Based on Atomically Thin Graphene-MoS_2 Heterostructures. *Sci. Rep.* **2014**, *4*, 3826.
30. Bertolazzi, S.; Krasnozhon, D.; Kis, A.; Nonvolatile Memory Cells Based On MoS_2/Graphene Heterostructures. *ACS Nano* **2013**, *7*, 3246–3252.
31. Kaasbjerg, K.; Thygesen, K. S.; Jacobsen, K. W. Phonon-limited Mobility In N-type Single-layer MoS_2 from First Principles. *Phys. Rev. B: Condens. Matter Mater. Phys.* **2012**, *85*, 115317.
32. Das, S.; Chen, H. Y.; Penumatcha, A. V.; Appenzeller, J. High Performance Multilayer MoS_2 Transistors with Scandium Contacts. *Nano Lett.* **2013**, *13*, 100–105.
33. Shi, H.; Pan, H.; Zhang, Y. W.; Yakobson, B. I. Quasiparticle Band Structures and Optical Properties of Strained Monolayer MoS_2 and WS_2. *Phys. Rev. B: Condens. Matter Mater. Phys.* **2013**, *87*, 155304.
34. Allain, A.; Kis, A. Electron and Hole Mobilities in Single-layer WSe_2. *ACS Nano* **2014**, *8*, 7180–7185.
35. Huang, J. K.; Pu, J.; Hsu, C. L.; Chiu, M. H.; Juang, Z. Y.; Chang, Y. H.; Chang, W. H.; Iwasa, Y.; Takenobu, T.; Li, L. J. Large-area Synthesis of Highly Crystalline WSe_2 Mono Layers and Device Applications. *ACS Nano* **2014**, *8*, 923–930.
36. Jones, A. M.; Yu, H. Y.; Ghimire, N. J.; Wu, S. F.; Aivazian, G.; Ross, J. S.; Zhao, B.; Yan, J. Q.; Mandrus, D. G.; Xiao, D.; *et al.* Optical Generation of Excitonic Valley Coherence in Monolayer WSe_2. *Nat. Nanotechnol.* **2013**, *8*, 634.
37. Yoshida, S.; Terada, Y.; Yokota, M.; Takeuchi, O.; Meray, Y.; Shigekawa, H. Direct Probing of Transient Photocurrent Dynamics in P-WSe_2 By Time-resolved Scanning Tunneling Microscopy. *Appl. Phys. Express* **2013**, *6*, 016601.
38. Novoselov, K. S.; Geim, A. K.; Morozov, S. V.; Jiang, D.; Zhang, Y.; Dubonos, S. V.; Grigorieva, I. V.; Firsov, A. A. Electric Field Effect In Atomically Thin Carbon Films. *Science* **2004**, *306*, 666–669.
39. Novoselov, K. S.; Geim, A. K.; Morozov, S. V.; Jiang, D.; Katsnelson, M. I.; Grigorieva, I. V.; Dubonos, S. V.; Firsov, A. A. Two-dimensional Gas of Massless Dirac Fermions in Graphene. *Nature* **2005**, *438*, 197–200.
40. Tonndorf, P.; Schmidt, R.; Bottger, P.; Zhang, X.; Borner, J.; Liebig, A.; Albrecht, M.; Kloc, C.; Gordan, O.; Zahn, D. R. T.; *et al.* Photoluminescence Emission and Raman Response of Monolayer MoS_2, $MoSe_2$, And WSe_2. *Opt. Express* **2013**, *21*, 4908–4916.
41. Zhao, W. J.; Ghorannevis, Z.; Chu, L. Q.; Toh, M. L.; Kloc, C.; Tan, P. H.; Eda, G. Evolution of Electronic Structure in Atomically Thin Sheets of WS_2 and WSe_2. *ACS Nano* **2013**, *7*, 791–797.
42. Lee, Y. H.; Zhang, X. Q.; Zhang, W. J.; Chang, M. T.; Lin, C. T.; Chang, K. D.; Yu, Y. C.; Wang, J. T. W.; Chang, C. S.; Li, L. J.; *et al.* Synthesis of Large-area MoS_2 Atomic Layers with Chemical Vapor Deposition. *Adv. Mater.* **2012**, *24*, 2320–2325.
43. Lee, Y. H.; Yu, L.; Wang, H.; Fang, W.; I Ling, X.; Shi, Y.; Lin, C. T.; Huang, J. K.; Chang, M. T.; Chang, C. S.; *et al.* Synthesis and Transfer of Single-layer Transition Metal Disulfides on Diverse Surfaces. *Nano Lett.* **2013**, *13*, 1852.
44. Liu, K. K.; Zhang, W. J.; Lee, Y. H.; Lin, Y. C.; Chang, M. T.; Su, C.; Chang, C. S.; Li, H.; Shi, Y. M.; Zhang, H.; *et al.* Growth of Large-area And Highly Crystalline MoS_2 Thin Layers on Insulating Substrates. *Nano Lett.* **2012**, *12*, 1538–1544.
45. Li, X. S.; Cai, W. W.; An, J. H.; Kim, S.; Nah, J.; Yang, D. X.; Piner, R.; Velamakanni, A.; Jung, I.; Tutuc, E.; *et al.* Large-area Synthesis of High-quality and Uniform Graphene Films on Copper Foils. *Science* **2009**, *324*, 1312–1314.
46. Korn, T.; Heydrich, S.; Hirmer, M.; Schmutzler, J.; Schuller, C. Low-temperature Photocarrier Dynamics in Monolayer MoS_2. *Appl. Phys. Lett.* **2011**, *99*, 102109.
47. Sundaram, R.; Engel, M.; Lombardo, A.; Krupke, R.; Ferrari, A.; H Avouris, P.; Steiner, M. Electroluminescence in Single Layer MoS_2. *Nano Lett.* **2013**, *13*, 1416–1421.
48. Wang, R.; Ruzicka, B. A.; Kumar, N.; Bellus, M. Z.; Chiu, H. Y.; Zhao, H. Ultrafast and Spatially Resolved Studies of Charge Carriers in Atomically Thin Molybdenum Disulfide. *Phys. Rev. B: Condens. Matter Mater. Phys.* **2012**, *86*, 045406.
49. Shi, H. Y.; Yan, R. S.; Bertolazzi, S.; Brivio, J.; Gao, B.; Kis, A.; Jena, D.; Xing, H. G.; Huang, L. B. Exciton Dynamics in Suspended Mono Layer And Few-layer MoS_2 2D Crystals. *ACS Nano* **2013**, *7*, 1072–1080.
50. Lee, C.; Yan, H.; Brus, L. E.; Heinz, T. F.; Hone, J.; Ryu, S. Anomalous Lattice Vibrations of Single- and Few-layer MoS_2. *ACS Nano* **2010**, *4*, 2695–2700.
51. Ulbricht, R.; Hendry, E.; Shan, J.; Heinz, T. F.; Bonn, M. Carrier Dynamics In Semiconductors Studied with Time-resolved Terahertz Spectroscopy. *Rev. Mod. Phys.* **2011**, *83*, 543–586.
52. Lloyd-Hughes, J.; Jeon, T.-I. A Review of the Terahertz Conductivity of Bulk and Nano-materials. *J. Infrared, Millimeter, Terahertz Waves* **2012**, *33*, 871.
53. Grabtchak, S. Y.; Cocivera, M. Contactless Microwave Study of Dispersive Transport in Thin Film CdSe. *J. Appl. Phys.* **1996**, *79*, 786–793.
54. Parkinson, P.; Joyce, H. J.; Gao, Q.; Tan, H. H.; Zhang, X.; Zou, J.; Jagadish, C.; Herz, L. M.; Johnston, M. B. Carrier Lifetime and Mobility Enhancement in Nearly Defect-free Core-shell Nanowires Measured Using Time-resolved Terahertz Spectroscopy. *Nano Lett.* **2009**, *9*, 3349–3353.
55. Joyce, H. J.; Wong-Leung, J.; Yong, C.; Docherty, C. J.; Paiman, S.; Gao, Q.; Tan, H. H.; Jagadish, C.; Lloyd-Hughes, J.; Herz, L. M.; *et al.* Ultra-low Surface Recombination Velocity in InP Nanowires Probed by Terahertz Spectroscopy. *Nano Lett.* **2012**, *12*, 5325–5330.
56. Joyce, H. J.; Docherty, C. J.; Gao, Q.; Tan, H. H.; Jagadish, C.; Lloyd-Hughes, J.; Herz, L. M.; Johnston, M. B. Electronic Properties of GaAs, Inas and InP Nanowires Studied by Terahertz Spectroscopy. *Nanotechnology* **2013**, *24*, 214006.
57. Fortin, E.; Raga, F. Excitons in Molybdenum-disulfide. *Phys. Rev. B: Solid State* **1975**, *11*, 905–912.
58. Yong, C. K.; Joyce, H. J.; Lloyd-Hughes, J.; Gao, Q.; Tan, H. H.; Jagadish, C.; Johnston, M. B.; Herz, L. M. Ultrafast Dynamics of Exciton Formation In Semiconductor Nanowires. *Small* **2012**, *8*, 1725–1731.
59. Docherty, C. J.; Lin, C.; Joyce, H. J.; Nicholas, R. J.; Herz, L. M.; Li, L.; Johnston, M. B. Extreme Sensitivity of Graphene Photoconductivity To Environmental Gases. *Nat. Commun.* **2012**, *3*, 1228.